# A two-fold quantum delayed-choice experiment in a superconducting circuit

K. Liu,<sup>1</sup> Y. Xu,<sup>1</sup> W. Wang,<sup>1</sup> Shi-Biao Zheng,<sup>2,\*</sup> Tanay Roy,<sup>3</sup> Suman Kundu,<sup>3</sup> Madhavi Chand,<sup>3</sup> A. Ranadive,<sup>3</sup> R. Vijay,<sup>3</sup> Y. P. Song,<sup>1</sup> L.-M. Duan,<sup>1,4,†</sup> and L. Sun<sup>1,‡</sup>

<sup>1</sup>Center for Quantum Information, Institute for Interdisciplinary Information Sciences, Tsinghua University, Beijing 100084, China

<sup>2</sup>Department of Physics, Fuzhou University, Fuzhou 350116, China

<sup>3</sup>Department of Condensed Matter Physics and Materials Science,

Tata Institute of Fundamental Research, Homi Bhabha Road, Mumbai 400005, India

<sup>4</sup>Department of Physics, University of Michigan, Ann Arbor, Michigan 48109, USA

We propose and experimentally demonstrate a two-fold quantum delayed-choice experiment where wave or particle nature of a superconducting interfering device can be post-selected twice after the interferometer. The wave-particle complementarity is controlled by a quantum which-path detector (WPD) in a superposition of its on and off states implemented through a superconducting cavity. The WPD projected to its on state records which-path information, which manifests the particle nature and destroys the interference associated with wave nature of the system. In our experiment, we can recover the interference signal through a quantum eraser even if the WPD has selected out the particle nature in the first round of delayed-choice detection, showing that a quantum WPD adds further unprecedented controllability to test of wave-particle complementarity through the peculiar quantum delayed-choice measurements.

Wave-particle duality is among the most fundamental properties of quantum mechanics. According to Bohr's principle of complementarity, a quantum system possesses complementary and mutually exclusive properties that cannot be observed at the same time [1-3]. Whether a quantum system behaves as a wave or a particle depends on the arrangement of measurement apparatus, as demonstrated by the delayed-choice experiment with a Mach-Zehnder (MZ) interferometer, in which the choice of inserting the second beam splitter BS<sub>2</sub> or not is made after the photon has entered the interferometer [4–9], as shown in Fig. 1a. When BS<sub>2</sub> is inserted, no path information is available so that the probability for detecting the photon at either outport depends upon the relative phase  $\varphi$  between the two paths, showing the interference effect. In the absence of BS<sub>2</sub>, detecting the photon at each outport unambiguously reveals which route the photon has travelled and no interference appears. The delayed-choice nature rules out the assumption that the photon could know beforehand what type of experimental apparatus it will be confronted with, and then behaves accordingly.

In a recent remarkable development, a quantum delayed-choice experiment was proposed in Ref. [10], where the action of BS<sub>2</sub> is controlled by a quantum ancilla: When the ancilla is in the state  $|0\rangle_a$ , BS<sub>2</sub> is removed; for the ancilla state  $|1\rangle_a$ , BS<sub>2</sub> is inserted. The process, in terms of quantum circuits [11], is shown in Fig. 1b, where the Hadamard gates H<sub>1</sub> and H<sub>2</sub> represent the corresponding beam splitters. When the ancilla is in a superposition of  $|0\rangle_a$  and  $|1\rangle_a$ , the wave-like and particle-like behaviors of the test system can be observed at the same time; these two complementary phenomena are encoded in the same output state and post-selected depending on the measured value of the ancilla. This proposal has been successfully demonstrated in experiments using photons

\*Electronic address: t96034@fzu.edu.cn †Electronic address: lmduanumich@gmail.com ‡Electronic address: luyansun@tsinghua.edu.cn [12–14] and other systems [15–17].

Here, we propose and experimentally demonstrate a two-fold quantum delayed-choice experiment by introducing a WPD in a superposition of its on and off states. As illustrated in Fig. 1c through a double-slit apparatus, when the WPD is in its on state  $|O\rangle$ , it collects the path information of the incoming quantum particle and labels its state to  $|O_1\rangle$  and  $|O_2\rangle$  corresponding to the two different paths 1 and 2 of the particle with wave functions  $\psi_1(\mathbf{r})$  and  $\psi_2(\mathbf{r})$ , respectively. When the WPD is in its off state  $|F\rangle$ , it does not record any information of the incoming particle. If the WPD starts at a superposition of its on and off states  $(|O\rangle + |F\rangle)/\sqrt{2}$ , the combined state of the WPD and the quantum particle becomes

$$|\Phi(\mathbf{r})\rangle = \frac{1}{2}[(|\psi_1(\mathbf{r})\rangle|O_1\rangle + |\psi_2(\mathbf{r})\rangle|O_2\rangle) + (|\psi_1(\mathbf{r})\rangle + |\psi_2(\mathbf{r})\rangle)|F\rangle].$$
(1)

If we measure the interference pattern of the quantum particle in the state  $|\Phi(\mathbf{r})\rangle$ , the interference fringes given by the cross terms  $\langle \psi_1(\mathbf{r})|\psi_2(\mathbf{r})\rangle + \langle \psi_2(\mathbf{r})|\psi_1(\mathbf{r})\rangle$  appear or disappear, depending on whether we post-project the WPD's state to the vector  $|F\rangle$  or the subspace O spanned by  $|O_1\rangle$  and  $|O_2\rangle$ . This gives a quantum delayed-choice experiment similar to Refs. 10, 12–17, but with the conceptual difference that this is enabled by a quantum WPD in a classical interferometer instead of by a quantum interferometer. This important difference leads to a distinction of the outcome: in our experiment, we can later erase the which-path information of the quantum particle [18-23] to recover the interference fringes even after we have projected the WPD to the "on" subspace O. This is achieved by measuring the WPD in the subspace O along the basis  $|\pm\rangle = (|O_1\rangle \pm |O_2\rangle)/\sqrt{2}$ , which fully restores the interference terms  $Re[\langle \psi_1(\mathbf{r}) | \psi_2(\mathbf{r}) \rangle]$ . In contrast, if we measure the WPD in the basis  $\{|O_1\rangle, |O_2\rangle\}$ , the interference fringe is completely lost. Therefore we can realize a two-fold quantum delayed-choice experiment, where we have two chances to choose the wave or particle behavior of the already detected quantum system, pushing test of wave-particle complementarity to an unprecedented level of controllability.

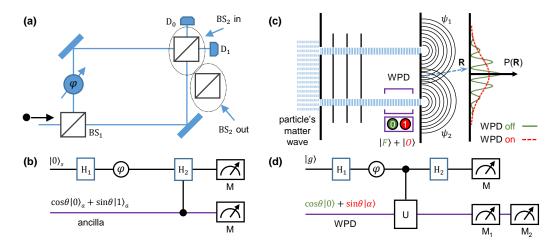


FIG. 1: Schematic diagrams of delayed-choice experiments with a two-path interferometer. (a) Wheeler's delayed-choice thought experiment. The decision of whether to insert BS<sub>2</sub> or not is delayed until after the photon has entered the interferometer. (b) Quantum delayed-choice experiment with a quantum beam splitter. Whether the second beam splitter-like (Hadamard) operation, H<sub>2</sub>, is applied or not depends upon whether the ancilla is in the state  $|1\rangle_a$  or  $|0\rangle_a$ . When the ancilla is in a superposition of these states, the test system can simultaneously behave as a wave and a particle. (c) Quantum delayed-choice experiment with a double-slit apparatus, where a WPD is placed in front of slit 2. When the WPD is switched on, it can store the which-path information of the incoming particle, destroying the interference. If the WPD is switched off, no path information is available. When the WPD is in a superposition of its on and off states, the wave and particle behaviors are encoded in the same output state. (d) Quantum delayed-choice experiment using a Ramsey interferometer, where a cavity acts as the WPD for a qubit's evolution in its quantum state space { $|g\rangle$ ,  $|e\rangle$ }. When the WPD contains a coherent field  $|\alpha\rangle$ , the conditional cavity  $\pi$ -phase shift U keeps track of the which-path information in the field's phase. For the vacuum state  $|0\rangle$ , which-path information is not collected. The qubit's particle and wave behaviors can be simultaneously observed by putting the WPD in a superposition state. Two successive measurements on the WPD enable implementation of a two-fold delayed-choice procedure.

We implement the two-fold quantum delayed-choice experiment with a superconducting Ramsey interferometer. The circuit diagram is shown in Fig. 1d, which is similar to that of a MZ interferometer, with the Hadamard gates  $H_1$  and  $H_2$  representing the beam splitters for the quantum state of a qubit, whose basis vectors  $|g\rangle$  and  $|e\rangle$  correspond to the two paths in the MZ interferometer. Here both  $H_1$  and  $H_2$  are implemented by a classical microwave pulse, corresponding to  $\pi/2$  rotations on the Bloch sphere. The qubit, initially in the state  $|g\rangle$ , is transformed to the superposition state  $(|g\rangle + |e\rangle)/\sqrt{2}$  by  $H_1$ . Then a relative phase shift between  $|g\rangle$  and  $|e\rangle$  is introduced to get the state  $(|g\rangle + e^{i\varphi}|e\rangle)/\sqrt{2}$ , mimicking the relative phase  $\varphi$  between the two interferometer arms. The WPD is represented by a cavity in the dispersive region, with its coupling to the qubit described by the Hamiltonian

$$H_e = \hbar \chi_{qs} a^{\dagger} a \otimes |e\rangle \langle e|, \qquad (2)$$

where  $\chi_{qs}$  denotes the coupling rate, and  $a^{\dagger}$  and a are the creation and the annihilation operators for the cavity mode. At interaction time  $\tau = \pi/\chi_{qs}$ , this coupling leads to a qubit-state-dependent  $\pi$ -phase shift:  $U = e^{i\pi a^{\dagger}a\otimes|e\rangle\langle e|}$  [24–26]. When the cavity is in the vacuum state  $|0\rangle$  (corresponding to the off state  $|F\rangle$  of the WPD), the qubit state is not affected by the cavity coupling operator U. After the Hadamard gate  $H_2$ , the probability for recording the qubit in the state  $|g\rangle$  is given by  $P_g = (1 - \cos \varphi)/2$ , which shows a perfect interference fringe with respect to the relative phase  $\varphi$ . However, if the cavity starts in a coherent state  $|\alpha\rangle$  (corresponding to the on state  $|O\rangle$  of the WPD), the coupling operator U evolves the qubit-cavity

system to the entangled state  $(|g\rangle |\alpha\rangle + e^{i\varphi} |e\rangle |-\alpha\rangle)/\sqrt{2}$ . The probability for getting the qubit in the state  $|g\rangle$  after  $H_2$  is given by  $P_g = (1-e^{-2|\alpha|^2}\cos\varphi)/2$ . When the overlap of the two labelling states  $|\alpha\rangle$  and  $|-\alpha\rangle$  is negligible, i.e.,  $e^{-2|\alpha|^2} \ll 1$ , the interference fringe disappears. In our experiment, the cavity is prepared in a superposition cat state

$$|\phi\rangle = \cos\theta |0\rangle + \sin\theta |\alpha\rangle, \tag{3}$$

and the probability for recording the qubit in state  $|g\rangle$  is given by

$$P_g \approx [\cos^2 \theta (1 - \cos \varphi) + \sin^2 \theta]/2, \tag{4}$$

where the two terms of  $P_g$  show respectively the wave behavior (interference) and the particle behavior (no interference) of the superconducting qubit.

The experimental implementation is based on a three-dimensional circuit quantum electrodynamics (circuit QED) architecture [27] (see Supplementary Material for details). The experiment starts with preparing the cavity in a coherent superposition of  $|0\rangle$  and  $|\alpha\rangle$  as in Eq. 3. The experimental pulse sequence (in Fig. 7) and detailed description are presented in the Supplementary Material. We experimentally generate such states with  $\alpha=2\sqrt{2}$ . For  $\theta=\pi/4$ , the fidelity  $F=\langle\phi|\rho_p|\phi\rangle=0.93$ , where  $\rho_p$  is the density operator of the produced cavity state (measured Wigner function is shown in Fig. 8 in the Supplementary Material). After creating the cat state, we sandwich the conditional  $\pi$ -phase shift gate U between two Hadamard gates  $H_1$  and  $H_2$  for the Ramsey interference measurement. In our experiment the tunable phase

shift  $\varphi$  is incorporated into the first Hadamard gate  $H_1$  by adjusting the phase of the corresponding microwave pulse. In Figs. 2a and 2b, we present the measured probability  $P_g$  as a function of  $\varphi$  for different values of  $\theta$ . As expected, the qubit exhibits a continuous transition between wave-like and particle-like behavior by varying  $\theta$  that determines the initial state of the WPD.

The essence of quantum delayed-choice experiments is that the quantum coherence of the measuring device excludes the possibility of the qubit knowing the measurement choice in advance. To verify the presence of the quantum coherence between the on and off states of the WPD, we perform the Wigner tomography after the Ramsey interference experiment [24-26, 28]. The Wigner function of a quantum harmonic oscillator, the quasiprobability distribution in phase space, contains all the information of the associated quantum state [29]. In Fig. 3 we present the reconstructed state of the cavity without post-selection on the qubit state (data conditional upon the qubit state  $|g\rangle$  and  $|e\rangle$  are presented in Fig. 9 in the Supplementary Material) for  $\theta = \pi/4$  and  $\varphi = \pi/2$ . As expected, the measured Wigner function (Fig. 3a) exhibits interference fringes, with alternate positive and negative values between 0 and  $\alpha$  ( $-\alpha$ ) in phase space, which are the signature of quantum coherence between  $|0\rangle$  and  $|\alpha\rangle$  ( $|-\alpha\rangle$ ). To further characterize this coherence, we display the density matrix (Fig. 3b) in the Hilbert space obtained from the measured Wigner function, where each term represents the modulus of the corresponding matrix element (without including the phase). The quantum coherence between  $|0\rangle$  and  $|\alpha\rangle$  ( $|-\alpha\rangle$ )

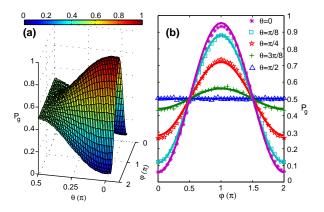


FIG. 2: Ramsey interference pattern. (a) Observation of continuous morphing between the qubit's particle and wave behaviors. The cavity, acting as the WPD, is initially prepared in the cat state of Eq. 3 with  $\alpha=2\sqrt{2}$ . The results clearly show that the measured Ramsey interference pattern of the qubit, characterized by  $P_g$  as a function of  $\varphi$ , depends upon the value of  $\theta$  that determines the state of the WPD. (b) Cuts in (a) for different values of  $\theta$ . Symbols are experimental data, which are in good agreement with the numerical simulations (solid lines) that take into account the experimental imperfections (except for measurement errors) including the qubit and cavity decoherence, the cross-Kerr interaction between the qubit and the cavity, and the self-Kerr interaction of the cavity. The standard deviation for each measured value is less than 0.01 and not shown in the figure.

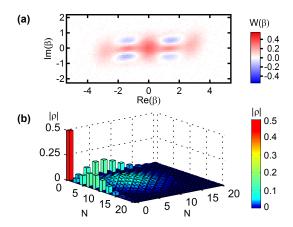


FIG. 3: Reconstruction of the cavity states after the second Ramsey pulse without selection on the qubit state. (a) The measured Wigner function and (b) density matrix for  $\alpha=2\sqrt{2}$ ,  $\theta=\pi/4$  and  $\phi=\pi/2$ . To clearly illustrate the quantum coherence between  $|0\rangle$  and  $|\alpha\rangle$  ( $|-\alpha\rangle$ ), we here only present the moduli of the density matrix elements in the Hilbert space, which are obtained from the corresponding measured Wigner function. The overlap (fidelity) between the measured density matrix  $\rho_m$  and ideal result  $\rho_i$ , defined as  $F=[Tr(\sqrt{\sqrt{\rho_i}\rho_m\sqrt{\rho_i}})]^2$ , is about 0.80; the infidelity is mainly due to the finite bandwidth of the  $\pi/2$  qubit pulses.

is manifested in the off-diagonal elements  $|\rho_{n,0}|$  and  $|\rho_{0,n}|$ , which are responsible for the observed interference fringes in the Wigner function [24]. These results unambiguously demonstrate that the qubit's behaviors with and without interference are observed with the same setup, where the WPD is in a quantum superposition of its on and off states.

To post-select the qubit's behavior, we examine whether the cavity is filled with a coherent field or is empty by using a conditional qubit rotation. Due to the dispersive qubit-cavity coupling, the qubit's transition frequency depends on the photon number of the cavity field, so that we can drive the qubit's transition conditional on the cavity being in a specific Fock state. After the Ramsey interference experiment we apply a  $\pi$  pulse to the qubit conditional on the cavity's vacuum state:  $R_{\pi,0}^Y = \exp\left[\frac{\pi}{2}|0\rangle\langle 0|\otimes (|e\rangle\langle g|-|g\rangle\langle e|)\right]$ . Since both  $|\alpha\rangle$  and  $|-\alpha\rangle$  are approximately orthogonal to  $|0\rangle$ , the qubit undergoes no transition for these two coherent state components. It should be noted that the coherent state  $|\alpha\rangle$  is not distinguished from  $|-\alpha\rangle$  after this procedure, that is, the whichpath information is not read out. In Fig. 4a we present the measured conditional probabilities  $P_{g;O}$  and  $P_{g;F}$  as functions of  $\varphi$ , which are defined as the probabilities for detecting the qubit in  $|g\rangle$  in the Ramsey interference experiment conditional on the measurement of the WPD's on state  $|\pm\alpha\rangle$  and off state  $|0\rangle$ , respectively. Here the on and off states have equal weighting, i.e.,  $\theta = \pi/4$ .  $P_{g;F}$  clearly manifests the qubit's interference behavior with a visibility of 0.89, while  $P_{g;O}$  almost shows no dependence on  $\varphi$ , as expected. Due to the imperfection of the conditional  $\pi$  pulse (Fig. 10g in the Supplementary Material), there is a small probability that  $|0\rangle$  is taken for  $|\pm\alpha\rangle$ ; this accounts for the residual interference effects (with a fringe contrast of 0.04) in  $P_{g;O}$ . These results clearly demon-

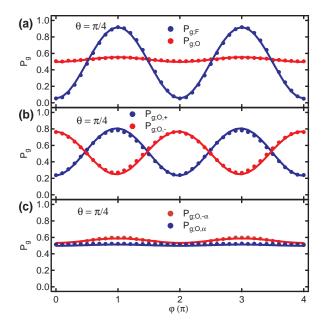


FIG. 4: Conditional Ramsey interference signals by post-selection on the WPD's state. (a) The probabilities  $P_{g;O}$  and  $P_{g;F}$ , as functions of  $\varphi$ , for detecting the qubit in the state  $|g\rangle$  in the Ramsey interference experiment conditional upon the post-selection of the cavity's states  $|\pm\alpha\rangle$  and  $|0\rangle$ , respectively. (b) The probabilities  $P_{g;O,+}$  and  $P_{g;O,-}$ , versus  $\varphi$ , for measuring the qubit in the state  $|g\rangle$ , conditional upon the measurement of even and odd parities of the WPD following the detection of the on state, respectively. (c) The probabilities  $P_{g;O,\alpha}$  and  $P_{g;O,-\alpha}$ , for detecting the qubit in the state  $|g\rangle$ , conditional upon post-selecting the WPD's on state and subsequently detecting the components  $|\alpha\rangle$  and  $|-\alpha\rangle$ , respectively. The parameters are  $\alpha=2\sqrt{2}$  and  $\theta=\pi/4$ . Dots represent experimental data with the standard deviation less than 0.01 and not shown, in excellent agreement with the numerical simulations (solid lines) based on the measured device parameters.

strate that the qubit's behavior depends upon the WPD's state; the quantum coherence of the on and off states, as shown in Fig. 3, excludes any model in which the choice corresponds to a classical variable that has been known in advance.

Unlike the previous quantum delayed-choice experiments [10, 12-17], here the which-path information associated with the qubit's particle-like behavior is not read out during the observation of the interference pattern; instead, it is stored in the field's phase. This path distinguishability can be erased: When we measure the cavity's parity, instead of distinguishing between  $|0\rangle$  and  $|\pm\alpha\rangle$ , and correlate the outcomes with the qubit's data, two complementary interference patterns appear (Fig. 11 in the Supplementary Material). More intriguingly, the quantum erasure [18-23] can be realized even after the particle-like behavior (the red line of Fig. 4a) has been post-selected, resulting in the restoration of the fringes. In Fig. 4b we plot the measured conditional probabilities  $P_{g;O,+}$  and  $P_{g;O,-}$  as functions of  $\varphi$ , defined as the probabilities for measuring the qubit in  $|g\rangle$  after H<sub>2</sub>, conditional on the detection of even and odd parities of the WPD following the post-selection of its on state, respectively. The fringe contrasts associated with  $P_{g;O,+}$  and  $P_{g;O,-}$  are 0.53 and 0.48, respectively. The imperfection of these conditional interference patterns is mainly due to the infidelity of the Hadamard gates used for qubit Ramsey interference and WPD parity discrimination, which is predominantly caused by cavity photons.

On the other hand, if we choose to read out the whichpath information by distinguishing between  $|\alpha\rangle$  and  $|-\alpha\rangle$ , the qubit shows no interference, as shown in Fig. 4c, where  $P_{g:O,\alpha}$ and  $P_{g;O,-\alpha}$  denote the probabilities to detect the state  $|g\rangle$  after H<sub>2</sub>, conditional on the post-selection of the WPD's on state and the subsequent measurement of  $|\alpha\rangle$  and  $|-\alpha\rangle$ , respectively. These two states can be distinguished by successively performing the cavity displacement  $D(-\alpha)$ , the conditional qubit  $\pi$  rotation  $R_{\pi,0}^{Y}$ , and the qubit state measurement. We note that thus obtained  $|-\alpha\rangle$  state is mixed up with the residual vacuum, resulting in a slight oscillation in  $P_{e:O,-\alpha}$  with a contrast of 0.07. This fringe contrast can be further reduced by performing additional operations  $D(\alpha)$  and  $R_{\pi,0}^{Y}$  and then measuring the qubit state to remove the residual vacuum. The deviation of  $P_{g;O,-\alpha}$  from 1/2 is mainly due to the qubit energy decay (see Supplementary Material).

The delayed-choice quantum eraser embedded in the quantum delayed-choice experiment is only enabled by employing the quantum properties of the WPD, significantly extending the concept of delayed-choice experiment. The two-fold delayed-choice procedure provides a clear demonstration that the behavior with or without interference is not a realistic property of the test system: It depends not only on the delayed choice of the WPD's state, but also on how we later measure the WPD and correlate the outcomes with the data of the test system.

In summary, we have proposed a two-fold quantum delayed-choice experiment which is enabled by using a WPD prepared in a superposition of its on and off states. We implemented the experiment in circuit QED, observing both behaviors with and without interference for a superconducting qubit in the same experiment by using a cavity in a cat state as the WPD. We confirmed the existence of quantum coherence between the on and the off states of the WPD, excluding interpretations of the results based on classical models. The quantum properties of the WPD allows erasure of the whichpath information associated with the post-selected particle-like behavior, implementing a two-fold delayed-choice procedure and illustrating the wave-particle complementarity in an unprecedented manner.

## Acknowledgments

We thank M. H. Devoret for helpful discussions. This work was supported by the Ministry of Science and the Ministry of Education of China through its grant to Tsinghua University, the National Natural Science Foundation of China under Grant Nos. 11374054 and 11474177, the Major State Basic Research Development Program of China under Grant No. 2012CB921601, and the 1000 Youth Fellowship program in

#### Appendix B: Pulse sequence and parameters

#### Appendix A: Experiment setup and device parameters

Our experiment is implemented with a three-dimensional circuit QED architecture [27] as shown in Fig. 5, where a single transmon qubit in a waveguide trench is dispersively coupled to two 3D cavities [25, 26], one cavity serving as the storage cavity and the other used to read out the qubit's state. The transmon qubit is fabricated on a c-plane sapphire (Al<sub>2</sub>O<sub>3</sub>) substrate with a double-angle evaporation of aluminum after a single electron-beam lithography step. The qubit has a transition frequency  $\omega_q/2\pi = 5.577$  GHz with an anharmonicity  $\alpha_q/2\pi=(\omega_{ge}-\omega_{ef})/2\pi=246$  MHz, an energy relaxation time  $T_1=9.5~\mu {\rm s}$ , a Ramsey time  $T_2^*=7.5~\mu {\rm s}$ , and a pure dephasing time  $T_{\phi}=12.4~\mu s$ . The sample is placed in a cryogen-free dilution refrigerator at a base temperature of about 10 mK. Even at the lowest base temperature, the qubit is measured to have a probability about 8.5% of being populated in the excited state  $|e\rangle$  in the steady state. The exact source for this excitation is unknown; it may be caused by stray infrared photons or other background noise leaking into the cavity. This excitation can be removed through an initialization measurement of the qubit state by post-selecting the projections of the system onto the ground state  $|g\rangle$  [30] (also see below). Both the storage and readout cavities are made of aluminum alloy 6061 with a frequency of 8.229 GHz and 7.292 GHz, respectively. The photon lifetimes in the storage and readout cavities are  $\tau_s = 66 \ \mu s$  and  $\tau_r = 44 \ ns$ , respectively. The dispersive couplings between the qubit and the storage (readout) cavity is  $\chi_{qs}/2\pi = -1.64 \text{ MHz} (\chi_{qr}/2\pi = -4.71 \text{ MHz})$ . For simplicity, we will refer to the storage cavity as "the cavity" henceforth. This cavity acts as the which-path detector (WPD) for the qubit in the Hilbert space.

The schematic of the measurement setup is shown in Fig. 6. We apply a Josephson parametric amplifier (JPA) [31, 32] operating in a double-pumped mode [33, 34] (red enclosed part in Fig. 6 shows the biasing circuit) as the first stage of amplification between the readout cavity at base and the high-electron-mobility-transistor amplifier at 4K. To minimize pump leakage into the readout cavity for a longer  $T_{\phi}$  time, we typically operate the JPA in a pulsed mode. This JPA allows for a high-fidelity and quantum non-demolition (QND) single-shot readout of the qubit state (see the section on "Readout Properties").

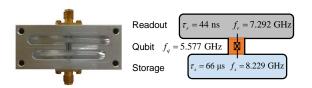


FIG. 5: **Experimental device.** Optical image and schematic of the device, where a transmon qubit is located in a trench and coupled to two 3D Al cavities.

The pulse sequence for the delayed-choice experiment is shown in Fig. 7. The whole process can be divided into four main parts: initialization of the system, creation of the superposition state of the WPD, Ramsey interference measurement of the qubit, and different measurements of the WPD's state. It is worth mentioning that except for the first two stochastic measurement parts, all the following measurement results are recorded and included in the analysis.

To get a high signal-to-noise ratio, the readout pulse is optimized to contain a few photons with a width of 240 ns. The first measurements in Figs. 7a and 7b are to purify the qubit state to  $|g\rangle$  by a post-selection. The pulses used to perform phase-space displacement for the cavity mode is chosen to be square-shaped with a width of 20 ns for a broad frequency span. The displacement amplitude is calibrated by a global Poisson distribution fitting of the probability of the first eight Fock states as a function of the arbitrary waveform generator DAC output [26]. This calibration also results in a background photon population  $n_{th} \sim 0.01$  in the cavity. In order to eliminate this thermal excitation, a cavity parity measurement is performed at the beginning of each experiment to purify the cavity state to  $|0\rangle$  (M2 in Figs. 7a and 7b).

The cavity parity measurement is achieved by sandwiching a conditional cavity  $\pi$ -phase shift between two qubit  $\pi/2$  rotations along the Y-axis on the Bloch sphere but with opposite rotation axes, denoted as  $R_{\pm\pi/2}^Y$  [24–26, 35]. To achieve a high-fidelity parity measurement, the  $R_{\pm\pi/2}^Y$  pulses used to perform these qubit rotations should equally cover as many number splitting peaks as possible without significantly exciting the second and higher excited state. As a good compromise, we use Gaussian envelope pulses truncated to  $4\sigma=8$  ns ( $\sigma_f=80$  MHz). We also apply the so-called "derivative removal by adiabatic gate" (DRAG) technique [36] to eliminate the possible qubit leakage to higher levels.

To distinguish a vacuum state  $|0\rangle$  and a coherent state  $|\alpha\rangle$  ( $\alpha=2\sqrt{2}$  in our experiment), we apply a conditional qubit  $\pi$  pulse  $R_{\pi,0}^Y$  which is effective only for a vacuum state. This pulse has a Gaussian envelope with  $\sigma \geq 100$  ns, allowing a good selectivity for  $\chi_{\sigma s}/2\pi=-1.64$  MHz.

# Appendix C: The cavity's cat state preparation and Wigner tomography

To create the WPD's coherent superposition state of  $|0\rangle$  and  $|\alpha\rangle$ , we first drive the cavity from  $|0\rangle$  to the coherent state  $|\alpha/2\rangle$  by performing a phase-space displacement, described by the operator  $D(\alpha/2) = \exp\left[(\alpha a^\dagger - \alpha^* a)/2\right]$ , and transform the qubit from  $|g\rangle$  to the superposition state  $\sin\theta\,|g\rangle + \cos\theta\,|e\rangle$ . Each of these operations is achieved by application of a classical microwave pulse. Then the qubit and cavity are entangled by the conditional  $\pi$ -phase shift gate U. After a subsequent Hadamard transformation, detection of the qubit in  $|g\rangle$  projects the cavity to the superposition state  $\cos\theta\,|-\alpha/2\rangle + \sin\theta\,|\alpha/2\rangle$ , which is then transformed

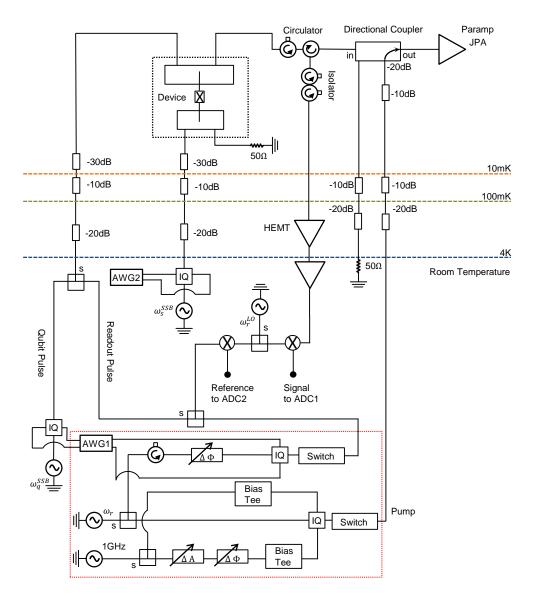


FIG. 6: Schematic of the measurement setup. A JPA operating in a double-pumped mode is used to read out the qubit state with a high fidelity and in a QND way. The part within the dashed red rectangle shows the biasing of the JPA.

by the displacement  $D(\alpha/2)$  to the state  $|\phi\rangle$  in Eq. 3 in the main text. We note that the superposition state of the WPD can also be realized deterministically as described in Ref. 25 but with a slightly lower fidelity. Therefore we only present data based on a measurement-induced superposition state of the WPD. Figure 8 shows the measured Wigner tomography of the WPD prepared in  $|\phi\rangle = \cos\theta \, |0\rangle + \sin\theta \, |\alpha\rangle$  (Eq. 3 in the main text) with  $\alpha = 2\sqrt{2}$  and  $\theta = \pi/4$ . The fidelity  $F = \langle \phi \, | \, \rho_p \, | \, \phi \rangle = 0.93$ , where  $\rho_p$  is the density operator of the produced cavity state.

To verify the presence of the quantum coherence between the on and off states of the WPD, we perform the Wigner tomography after the Ramsey interference experiment [24–26, 28]. In Figs. 9a and 9b we present the reconstructed states of the cavity conditional on the qubit being measured in  $|g\rangle$  and  $|e\rangle$  after H<sub>2</sub>, respectively, all for  $\theta = \pi/4$  and  $\varphi = \pi/2$ .

As expected, each of the measured Wigner functions (upper row) exhibits interference fringes, with alternate positive and negative values between 0 and  $\alpha$  ( $-\alpha$ ) in phase space, which are the signature of quantum coherence between  $|0\rangle$  and  $|\alpha\rangle$  ( $|-\alpha\rangle$ ). This is also manifested in the off-diagonal elements  $|\rho_{n,0}|$  and  $|\rho_{0,n}|$  in the density matrices (lower row) in the Hilbert space obtained from the measured Wigner functions. These results unambiguously demonstrate that the qubit's behaviors with and without interference are observed with the same setup, where the WPD is in a quantum superposition of its on and off states.

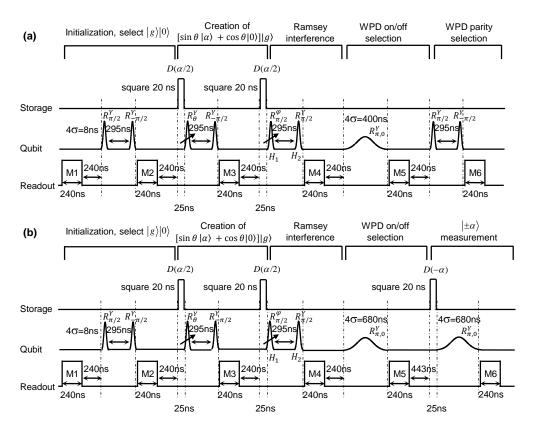


FIG. 7: Schematic of the pulse sequences in the experiments. The whole experiment can be divided into four main parts: 1) initialization of the system to  $|g\rangle|0\rangle$  by post-selecting results of the qubit measurement and the cavity parity measurement; 2) creation of an arbitrary superposition state of the WPD,  $\sin\theta\,|\alpha\rangle + \cos\theta\,|0\rangle$ ; 3) Ramsey interference measurement of the qubit with variable phase  $\varphi$  in the first  $\pi/2$  pulse  $R_{\pi/2}^{\varphi}$ ; 4) measurements of the WPD's state: on/off state post-selection of the WPD (gives  $P_{g;O}$  and  $P_{g;F}$ , Fig. 4a in the main text), and, under the on state, (a) the parity measurement of the WPD (gives  $P_{g;O,+}$  and  $P_{g;O,-}$ , Fig. 4b in the main text); (b) the discrimination of  $|\alpha\rangle$  and  $|-\alpha\rangle$  states (gives  $P_{g;O,-\alpha}$  and  $P_{g;O,-\alpha}$ , Fig. 4c in the main text).

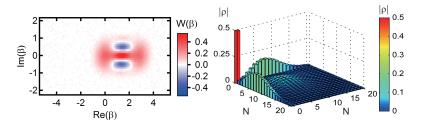


FIG. 8: **Tomography of initial cavity state.** Measured Wigner function (left) and density matrix (right) of the cavity initially prepared in the cat state of  $|\phi\rangle = \cos\theta \, |0\rangle + \sin\theta \, |\alpha\rangle$  (Eq. 3 in the main text) with  $\alpha = 2\sqrt{2}$  and  $\theta = \pi/4$ . The fidelity  $F = \langle \phi \, | \, \rho_p \, | \, \phi \rangle = 0.93$ , where  $\rho_p$  is the density operator of the produced cavity state.

## Appendix D: Readout properties

The readout properties of the qubit and cavity photon state are first characterized as shown in Fig. 10. Because we initialize the qubit to the ground state  $|g\rangle$  and use pulses with DRAG to minimize the leakage to levels higher than the first excited state  $|e\rangle$ , we do not distinguish the levels higher than  $|e\rangle$  in the readout. We adjust the phase difference between the JPA readout signal and the pump in such a way that  $|g\rangle$  and  $|e\rangle$  states can be distinguished with optimal contrast. Figure 10a shows

the histogram of the qubit readout. The histogram is clearly bimodal and well separated. A threshold  $V_{th}=0$  is chosen to digitize the readout signal to +1 and -1 for  $|g\rangle$  and  $|e\rangle$  states, respectively.

The purification of the qubit to  $|g\rangle$  is achieved by a QND measurement of the qubit state; the subsequent measurement shows that the probability of the qubit being populated in  $|g\rangle$  is as high as 0.996 after the initial purification (dashed histogram in Fig. 10a). Figure 10c shows the basic qubit readout properties with the cavity left in vacuum. The readout fidelity of the

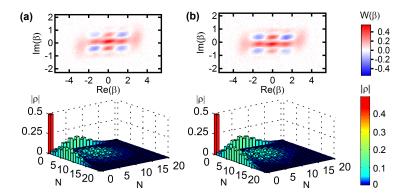


FIG. 9: Reconstruction of the cavity states after the second Ramsey pulse. (a) Conditional upon the qubit state  $|g\rangle$ . (b) Conditional upon the  $|e\rangle$  state. The measured Wigner functions and density matrices are shown in the upper and lower rows, respectively, all for  $\alpha = 2\sqrt{2}$ ,  $\theta = \pi/4$  and  $\varphi = \pi/2$ . To clearly illustrate the quantum coherence between  $|0\rangle$  and  $|\alpha\rangle$  ( $|-\alpha\rangle$ ), we here only present the moduli of the density matrix elements in the Hilbert space, which are obtained from the corresponding measured Wigner functions. The overlap (fidelity) between the measured density matrix  $\rho_m$  and ideal result  $\rho_i$ , defined as  $F = [Tr(\sqrt{\sqrt{\rho_i}\rho_m\sqrt{\rho_i}})]^2$ , is about 0.80 for each case; the infidelities are mainly due to the finite bandwidth of the  $\pi/2$  qubit pulses.

qubit state  $|e\rangle$ , prepared by properly pumping the selected  $|g\rangle$  state (Fig. 10d), is 0.943. The readout errors are mainly due to the  $T_1$  process during the waiting time after the initialization measurement (240 ns) and during the readout time (240 ns).

Figure 10e shows the readout property of the cavity parity state. Due to the decoherence of the qubit, there is a slight difference (typically a couple of percent) between the cases starting with  $|g\rangle$  or  $|e\rangle$ . Here we neglect this small difference. The cat states with  $\alpha=2\sqrt{2}$  and the vacuum state  $|0\rangle$  are created through pulse sequences in Fig. 7 with the appropriate  $\theta$  and  $\varphi$ . The parity readout infidelity for the cat states is mainly due to the loss of effectiveness of the  $\pi/2$  pulses and the qubit decoherence during the parity measurement (Fig. 10f).

Figure 10g shows the selectivity property of the Gaussian  $\pi$  pulse  $R_{\pi,0}^Y$  with  $\sigma=100$  ns for distinguishing between the cavity states  $|\pm\alpha\rangle$  and  $|0\rangle$  (Fig. 10h). For  $\alpha=2\sqrt{2}$ , the difference between the readout fidelities of the cavities state  $|\pm\alpha\rangle$  associated with the qubit states  $|g\rangle$  and  $|e\rangle$  is due to the decay of  $|e\rangle$  during the long duration of this selective  $\pi$  pulse. Here we note that the cavity states  $|\pm\alpha\rangle$  and  $|0\rangle$  are created with and without a direct displacement  $D(\pm\alpha)$ . The fidelities will be a few percent lower if we create  $|\pm\alpha\rangle$  and  $|0\rangle$  states using the sequence in Fig. 7 with  $\theta=\pi/2$  and 0, respectively.

### Appendix E: Quantum erasure

In our quantum delayed-choice experiment, the which-path information associated with the qubit's particle-like behavior is encoded in the phase of the cavity field, which can be erased by performing the parity measurement on the cavity even after the qubit has been detected [18–23]. To see this clearly, we rewrite the output state of the total system after H<sub>2</sub> in the

Ramsey interference measurement as

$$|\psi\rangle = |\phi_{+}\rangle \left(\cos\theta |0\rangle + \frac{\sin\theta |\Phi_{+}\rangle}{\sqrt{2}}\right) + |\phi_{-}\rangle \frac{\sin\theta |\Phi_{-}\rangle}{\sqrt{2}},$$
(F1)

where  $|\phi_{\pm}\rangle=rac{1}{2}[(|g\rangle+|e\rangle)\pm e^{i\phi}(|e\rangle-|g\rangle)]$  and  $|\Phi_{\pm}\rangle=$  $\frac{1}{\sqrt{2}}(|\alpha\rangle \pm |-\alpha\rangle)$ . This implies that the probability for finding the qubit being in the state  $|g\rangle$  conditional upon the parity of the WPD being even or odd is  $P_{g;\pm} = \frac{1}{2}(1 \mp \cos\varphi)$ , which exhibits interference fringes with a unit contrast. The results have a simple explanation. Each of the two coherent states  $|\alpha\rangle$ and  $|-\alpha\rangle$  consists of both even- and odd-parity components  $|\Phi_{+}\rangle$  and  $|\Phi_{-}\rangle$  with the same weighting; the which-path information is encoded in the states  $|\alpha\rangle$  and  $|-\alpha\rangle$ , other than in  $|\Phi_{+}\rangle$  and  $|\Phi_{-}\rangle$ . When the cavity is detected in a definite parity state, it is impossible to determine whether it comes from  $|\alpha\rangle$  or from  $|-\alpha\rangle$ , erasing the which-path information. Fig. 11 displays the measured conditional probabilities  $P_{g;+}$ and  $P_{g,-}$  as functions of  $\varphi$  for  $\theta = \pi/4$ , which are defined as the probabilities for detecting the qubit in the state  $|g\rangle$  after H<sub>2</sub>, conditional upon the detection of even and odd parities of the WPD, respectively. The measurement sequence is identical to Fig. 7a except for removing the "WPD on/off selection" (M5). As expected,  $P_{g;+}$  and  $P_{g;-}$  exhibits complementary interference patterns, that is, the maxima in  $P_{g;+}$  correspond to the minima in  $P_{g;-}$ . The fringe visibilities associated with these two interference patterns are 0.82 and 0.50, respectively. The reduction of the fringe contrast, compared to the ideal case, can be explained as follows. Due to the finite bandwidth of the pulses used to perform the qubit  $\pi/2$  rotations in the frequency domain, when the photon number of the cavity increases, the fidelity of these rotations decreases, resulting in the reduction of the parity measurement fidelity. The vacuum state constitutes the main contribution to the even parity component, so that the Hadamard gates operate more effectively for the even parity than for the odd parity, which accounts for the result that the fringe contrast of  $P_{g;+}$  is higher than that of

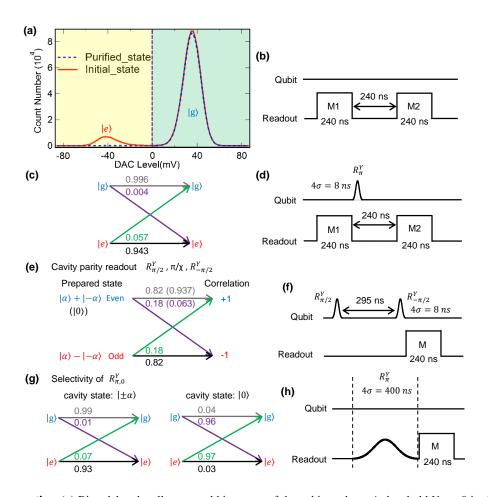


FIG. 10: **Readout properties.** (a) Bimodal and well-separated histogram of the qubit readout. A threshold  $V_{th}=0$  is chosen to digitize the readout signal. The solid line corresponds to the case without the qubit purification measurement, showing the qubit has an 8.5% probability of being populated in  $|e\rangle$  state, while the dashed line represents the result after the qubit has been purified. (b) The measurement pulse sequence used in **a**. (c) Basic qubit readout matrix with the cavity left in vacuum. The readout errors are mainly due to the  $T_1$  process. (d) The measurement pulse sequence used in **c**. (e) Readout property of the cavity parity state. The parity readout infidelity for the WPD's on state  $(\alpha=2\sqrt{2})$  is mainly due to the loss of effectiveness of the  $\pi/2$  pulses and the qubit decoherence. (f) The pulse sequence for the parity measurement. (g) The selectivity property of the Gaussian  $\pi$  pulse  $R_{\pi,0}^Y$  with  $\sigma=100$  ns. The difference between the readout fidelities of the cavity state  $|\pm\alpha=\pm2\sqrt{2}\rangle$  associated with the qubit states  $|g\rangle$  and  $|e\rangle$  is due to the decay of  $|e\rangle$  during the long duration of this selective  $\pi$  pulse. (h) The pulse sequence used in g.

 $P_{g;-}$ .

# Appendix F: Analysis of errors in marking the which-path information

As has been shown in the main text, the procedure for marking the which-path information consists of a displacement operation  $D(-\alpha)$ , a conditional qubit  $\pi$  rotation  $R_{\pi,0}^Y$ , and a qubit state readout (Fig. 7b). Due to the dispersive qubit-cavity coupling, the cavity frequency depends on the qubit state, so that the cavity coherent states associated with the qubit state  $|e\rangle$  are asynchronous with those associated with  $|g\rangle$ . To make the coherent state discrimination independent of the qubit state, the displacement operation is delayed in such a way that the coherent states associated with different qubit states re-synchronize when the displacement pulse is applied.

To meet the required long delay time, we choose  $4\sigma = 680$  ns for  $R_{\pi,0}^Y$ , which also gives a better selectivity between  $|0\rangle$  and  $|\alpha\rangle$ . The waiting time after the measurement is properly adjusted by checking the alignment of centers of the coherent states in the phase space associated with  $|g\rangle$  and  $|e\rangle$  states.

Without considerations of experimental imperfections, neither conditional qubit  $\pi$  rotation  $R_{\pi,0}^Y$  can cause the qubit state to flip when the cavity is in the coherent state  $|-\alpha\rangle$  after the Ramsey interference experiment. Therefore, the conditional probability  $P_{g;O,-\alpha}$  in Fig. 4c of the main text is

$$P_{g;O,-\alpha} = \frac{P_{g,g,g}}{P_{g,g,g} + P_{e,e,e}},$$
 (F1)

where  $P_{g,g,g}(P_{e,e,e})$  is the probability that the qubit is measured to be in  $|g\rangle$  ( $|e\rangle$ ) state during all the processes in the last three measurements (M4-M6) in Fig. 7b, including observa-

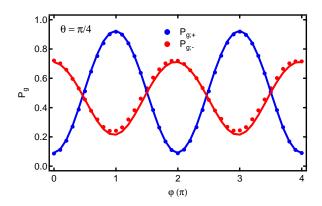


FIG. 11: Conditional Ramsey interference patterns based on the cavity parity measurement.  $P_{g;+}$  and  $P_{g;-}$  represent the probabilities as a function of  $\varphi$  for detecting the qubit in the state  $|g\rangle$  in the Ramsey interference experiment conditional upon the detection of even and odd parities of the cavity field, respectively. Due to the erasure of the which-path information, the interferences reappear. Dots are experimental data with the standard deviation less than 0.01 and not shown, in good agreement with the numerical simulations (solid lines) based on the measured device parameters.

tion of the Ramsey interference pattern, post-selection of the WPD's action, and distinction between  $|\alpha\rangle$  and  $|-\alpha\rangle$ . The ideal values of  $P_{g,g,g}$  and  $P_{e,e,e}$  are both equal to 1/8. However, due to the qubit energy decay,  $P_{e,e,e}$  becomes smaller so that  $P_{g;O,-\alpha} > 1/2$ . This decay (on average about 1.2  $\mu$ s long) mainly occurs during the long duration for performing

the conditional qubit  $\pi$  rotation, the measurement time, and the delay for re-synchronizing the joint qubit-cavity state. The measured average value of  $P_{g;O,-\alpha}$  is 0.56, in good agreement with the expected one taking into account the qubit decay:  $P_{g,g,g}/(P_{g,g,g}+P_{e,e,e})\approx 1/(1+e^{-1.2\times2/9.5})=0.56$ . The small fringe contrast mainly comes from the residual vacuum which can be further excluded by performing additional operations  $D(\alpha)$  and  $R_{\pi,0}^{\gamma}$  and then measuring the qubit state.

On the other hand, when the cavity is measured to be in the coherent state  $|\alpha\rangle$  after the coherent state discrimination, the corresponding conditional probability  $P_{g;O,\alpha}$  shows almost no oscillation (the fringe contrast is less than 0.01). The reason is that  $|\alpha\rangle$  state is nearly perfectly distinguished from  $|-\alpha\rangle$  and  $|0\rangle$  in this process. As a result,  $P_{g;O,\alpha}$  is given by

$$P_{g;O,\alpha} = \frac{P_{g,g,e}}{P_{g,g,e} + P_{e,e,g}},$$
 (F2)

where  $P_{g,g,e}$  ( $P_{e,e,g}$ ) denotes the probability that the qubit is measured to be in  $|g\rangle$  ( $|e\rangle$ ) state during the observation of the Ramsey interference pattern and the subsequent post-selection of the WPD's action, and in  $|e\rangle$  ( $|g\rangle$ ) during the procedure for distinguishing between  $|\alpha\rangle$  and  $|-\alpha\rangle$  (M4-M6 in Fig. 7b). The measured average value of  $P_{g;O,\alpha}=0.52$ , with the small deviation from 0.5 mainly coming from the qubit decay during the post-selection of the WPD's action ( $\approx 1/(1+e^{-1/9.5})=0.53$ ). We note that the cavity state  $|\alpha\rangle$  is transformed to  $|0\rangle$  during the coherent state discrimination, so that the readout fidelities of this cavity state associated with the qubit states  $|e\rangle$  and  $|g\rangle$  are almost the same.

- [1] N. Bohr, in *Quantum theory and measurement*, edited by J. A. Wheeler and W. H. Zurek (Princeton Univ. Press, Princeton, NJ, 1984), pp. 9–49.
- [2] B.-G. Englert, Phys. Rev. Lett. 77, 2154 (1996).
- [3] S. Dürr, T. Nonn, and G. Rempe, Nature 395, 33 (1998).
- [4] J. A. Wheeler, in *Quantum Theory and Measurement*, edited by J. A. Wheeler and W. H. Zurek (Princeton Univ. Press, Princeton, NJ, 1984), pp. 182–213.
- [5] X. S. Ma, J. Kofler, and A. Zeilinger, Rev. Mod. Phys. 88, 015005 (2016).
- [6] T. Hellmuth, H. Walther, A. Zajonc, and W. Schleich, Phys. Rev. A 35, 2532 (1987).
- [7] B. J. Lawson-Daku, R. Asimov, O. Gorceix, C. Miniatura, J. Robert, and J. Baudon, Phys. Rev. A 54, 5042 (1996).
- [8] V. Jacques, E. Wu, F. Grosshans, F. Treussart, P. Grangier, A. Aspect, and J.-F. Roch, Science 315, 966 (2007).
- [9] A. G. Manning, R. I. Khakimov, R. G. Dall, and A. G. Truscott, Nat. Phys. 11, 539 (2015).
- [10] R. Ionicioiu and D. R. Terno, Phys. Rev. Lett. 107, 230406 (2011).
- [11] M. A. Nielsen and I. L. Chuang, Quantum Computation and Quantum Information (Cambridge Univ. Press, 2000).
- [12] J.-S. Tang, Y.-L. Li, X.-Y. Xu, G.-Y. Xiang, C.-F. Li, and G.-C. Guo, Nat. Photon. 6, 600 (2012).
- [13] A. Peruzzo, P. Shadbolt, N. Brunner, S. Popescu, and J. L. O'Brien, Science 338, 634 (2012).

- [14] F. Kaiser, T. Coudreau, P. Milman, D. B. Ostrowsky, and S. Tanzilli, Science 338, 637 (2012).
- [15] S. S. Roy, A. Shukla, and T. S. Mahesh, Phys. Rev. A 85, 022109 (2012).
- [16] R. Auccaise, R. M. Serra, J. G. Filgueiras, R. S. Sarthour, I. S. Oliveira, and L. C. Céleri, Phys. Rev. A 85, 032121 (2012).
- [17] S.-B. Zheng, Y.-P. Zhong, K. Xu, Q.-J. Wang, H. Wang, L.-T. Shen, C.-P. Yang, J. M. Martinis, A. N. Cleland, and S.-Y. Han, Phys. Rev. Lett. 115, 260403 (2015).
- [18] M. O. Scully and K. Drühl, Phys. Rev. A 25, 2208 (1982).
- [19] M. O. Scully, B. G. Englert, and H. Walther, Nature 351, 111 (1991).
- [20] C. C. Gerry, Phys. Rev. A 53, 1179 (1996).
- [21] T. J. Herzog, P. G. Kwiat, H. Weinfurter, and A. Zeilinger, Phys. Rev. Lett. 75, 3034 (1995).
- [22] Y.-H. Kim, R. Yu, S. P. Kulik, Y. Shih, and M. O. Scully, Phys. Rev. Lett. 84, 1 (2000).
- [23] X. S. Ma, J. Kofler, A. Qarry, N. Tetik, T. Scheidl, R. Ursin, S. Ramelow, T. Herbst, L. Ratschbacher, A. Fedrizzi, et al., Proc. Natl. Acad. Sci. USA 110, 1221 (2013).
- [24] S. Deléglise, I. Dotsenko, C. Sayrin, J. Bernu, M. Brune, J. M. Raimond, and S. Haroche, Nature 455, 510 (2008).
- [25] B. Vlastakis, G. Kirchmair, Z. Leghtas, S. E. Nigg, L. Frunzio, S. M. Girvin, M. Mirrahimi, M. H. Devoret, and R. J. Schoelkopf, Science 342, 607 (2013).
- [26] L. Sun, A. Petrenko, Z. Leghtas, B. Vlastakis, G. Kirchmair,

- K. M. Sliwa, A. Narla, M. Hatridge, S. Shankar, J. Blumoff, et al., Nature **511**, 444 (2014).
- [27] H. Paik, D. I. Schuster, L. S. Bishop, G. Kirchmair, G. Catelani, A. P. Sears, B. R. Johnson, M. J. Reagor, L. Frunzio, L. Glazman, et al., Phys. Rev. Lett. 107, 240501 (2011).
- [28] L. G. Lutterbach and L. Davidovich, Phys. Rev. Lett. 78, 2547 (1997).
- [29] W. P. Schleich, Quantum optics in phase space (Wiley-VCH, 2001).
- [30] D. Ristè, J. G. van Leeuwen, H.-S. Ku, K. W. Lehnert, and L. DiCarlo, Phys. Rev. Lett. 109, 050507 (2012).
- [31] M. Hatridge, R. Vijay, D. H. Slichter, J. Clarke, and I. Siddiqi, Phys. Rev. B 83, 134501 (2011).

- [32] T. Roy, S. Kundu, M. Chand, V. A. M., A. Ranadive, N. Nehra, M. P. Patankar, J. Aumentado, A. A. Clerk, and R. Vijay, Appl. Phys. Lett. 107, 262601 (2015).
- [33] A. Kamal, A. Marblestone, and M. H. Devoret, Phys. Rev. B 79, 184301 (2009).
- [34] K. W. Murch, S. J. Weber, C. Macklin, and I. Siddiqi, Nature 502, 211 (2013).
- [35] P. Bertet, A. Auffeves, P. Maioli, S. Osnaghi, T. Meunier, M. Brune, J. M. Raimond, and S. Haroche, Phys. Rev. Lett. 89, 200402 (2002).
- [36] F. Motzoi, J. M. Gambetta, P. Rebentrost, and F. K. Wilhelm, Phys. Rev. Lett. 103, 110501 (2009).